

Evaluation of Integral Depth-dose Curves in Proton Pencil Beam Scanning
using Plane-parallel Ionization Chambers



A Thesis Submitted in Partial Fulfillment of the Requirements
for the Degree of Master of Science in Medical Physics

Department of Radiology

FACULTY OF MEDICINE

Chulalongkorn University

Academic Year 2021

Copyright of Chulalongkorn University

การประเมินปริมาณรังสีสะสมตามความลึกในอนุภาคโปรตอนแบบสแกนขนาดเล็ก
ด้วยหัววัดรังสีไอออนไนเซชันแบบขนาน



วิทยานิพนธ์นี้เป็นส่วนหนึ่งของการศึกษาตามหลักสูตรปริญญาวิทยาศาสตรมหาบัณฑิต
สาขาวิชาฟิสิกส์การแพทย์ ภาควิชารังสีวิทยา
คณะแพทยศาสตร์ จุฬาลงกรณ์มหาวิทยาลัย
ปีการศึกษา 2564
ลิขสิทธิ์ของจุฬาลงกรณ์มหาวิทยาลัย

ภัทรพร ฐาศศิรั : การประเมินปริมาณรังสีสะสมตามความลึกในอนุภาคโปรตอนแบบสแกนขนาดเล็กด้วยหัววัดรังสีไอออนไนเซชันแบบขนาน. (Evaluation of Integral Depth-dose Curves in Proton Pencil Beam Scanning using Plane-parallel Ionization Chambers) อ.ที่ปรึกษาหลัก : อ. ดร.สรจรส อุณหศิริ

การฉายรังสีด้วยอนุภาคโปรตอนเป็นรูปแบบการรักษาด้วยรังสีขั้นสูง โดยมีข้อดีคือสามารถลดผลข้างเคียงและเพิ่มโอกาสในการควบคุมโรคในผู้ป่วยโรคมะเร็ง ซึ่งหนึ่งในพารามิเตอร์ที่สำคัญที่จำเป็นต้องทำการวัดและใส่ข้อมูลลงในระบบวางแผนการรักษา เพื่อใช้ในการคำนวณปริมาณรังสีก่อนนำอนุภาคโปรตอนมาใช้ในการรักษาผู้ป่วยคือปริมาณรังสีสะสมตามความลึก และเนื่องจากมีปริมาณรังสีต่ำอยู่รอบ ๆ ลำรังสีหลัก จึงจำเป็นต้องใช้หัววัดรังสีไอออนไนเซชันแบบขนานที่มีขนาดใหญ่ เพื่อที่จะได้วัดปริมาณรังสีได้ครอบคลุมทั้งหมด โดยวัตถุประสงค์ของงานวิจัยนี้คือ เพื่อประเมินปริมาณรังสีสะสมตามความลึกและประสิทธิภาพในการวัดปริมาณรังสีที่ความลึกระดับกลาง เมื่อวัดด้วยหัววัดรังสีไอออนไนเซชันแบบขนานที่มีขนาดเส้นผ่านศูนย์กลางแตกต่างกันในอนุภาคโปรตอนแบบสแกนขนาดเล็ก เริ่มจากวัดปริมาณรังสีสะสมตามความลึกของอนุภาคโปรตอนพลังงาน 70 ถึง 220 MeV ด้วย Bragg peak chamber ชนิด 34070 ที่มีขนาดเส้นผ่านศูนย์กลาง 8 เซนติเมตร และชนิด 34089 ขนาดเส้นผ่านศูนย์กลาง 15 เซนติเมตร, Giraffe ขนาดเส้นผ่านศูนย์กลาง 12 เซนติเมตร และ PeakFinder ขนาดเส้นผ่านศูนย์กลาง 8 เซนติเมตร จากนั้นประเมินประสิทธิภาพในการวัดปริมาณรังสี โดยคำนวณสัดส่วนปริมาณรังสีสะสมตามความลึกระหว่างหัววัดรังสีไอออนไนเซชันแบบขนานที่มีขนาดเส้นผ่านศูนย์กลางแตกต่างกัน ผลการศึกษาพบว่าที่ความลึกระดับกลางของอนุภาคโปรตอนพลังงาน 130, 150, 190 และ 220 MeV เส้นกราฟปริมาณรังสีสะสมตามความลึกของ Bragg peak chamber ชนิด 34089 อยู่สูงที่สุด รองลงมาคือเส้นกราฟของ Giraffe, Bragg peak chamber ชนิด 34070 และ PeakFinder ตามลำดับ สำหรับประสิทธิภาพในการวัดปริมาณรังสีพบว่า Bragg peak chamber ชนิด 34089 สามารถวัดปริมาณรังสีได้มากกว่า 3.8%, 6.1% และ 3.1% เมื่อเทียบกับ Bragg peak chamber ชนิด 34070, PeakFinder และ Giraffe ตามลำดับ โดยสรุปคือหัววัดรังสีไอออนไนเซชันแบบขนานที่มีขนาดเส้นผ่านศูนย์กลางใหญ่ขึ้นสามารถเพิ่มประสิทธิภาพในการวัดปริมาณรังสีได้ โดยเฉพาะอย่างยิ่งที่ความลึกระดับกลางและอนุภาคโปรตอนพลังงานสูง

สาขาวิชา ฟิสิกส์การแพทย์

ลายมือชื่อนิสิต

ปีการศึกษา 2564

ลายมือชื่อ อ.ที่ปรึกษาหลัก

6370039930 : MAJOR MEDICAL PHYSICS

KEYWORD: Proton therapy, Pencil beam scanning, Integral depth dose

Phatthraporn Thasasi : Evaluation of Integral Depth-dose Curves in Proton Pencil Beam Scanning using Plane-parallel Ionization Chambers. Advisor: Sornjarod Oonsiri, Ph.D.

Proton therapy is an advanced form of radiation therapy treatment that can potentially decrease side effects and increase tumor control probability. The integral depth-dose curve is an essential parameter that has to be determined and introduced into the proton treatment planning system for the dose calculation. Besides the halo, the integral depth-dose curve measurements should be performed with a large-diameter plane-parallel ionization chamber. The purpose of this research is to determine the integral depth-dose curves and assess the geometrical collection efficiency at intermediate depths of different detector diameters in proton pencil beam scanning. The integral depth-dose curves with a proton energy range of 70 to 220 MeV were measured using Bragg peak chambers type 34070 with 8 cm diameter and 34089 with 15 cm diameter (PTW, Germany), multi-layer ionization chamber with 12 cm diameter (Giraffe, IBA dosimetry), and PeakFinder with 8 cm diameter (PTW, Germany). To assess the geometrical collection efficiency, the ratios of a depth-dose curve from two different chambers were investigated. The results found that at intermediate depths of 130, 150, 190, and 220 MeV, PTW Bragg peak chamber type 34089 provided the highest integral depth-dose curves followed by IBA Giraffe, PTW Bragg peak chamber type 34070, and PTW PeakFinder. Besides that PTW Bragg peak chamber type 34089 had increased geometrical collection efficiency up to 3.8%, 6.1%, and 3.1% compared to PTW Bragg peak chamber type 34070, PTW PeakFinder, and IBA Giraffe, respectively. In conclusion, a larger plane-parallel ionization chamber could increase the geometrical collection efficiency of the detector, especially at intermediate depths and high-energy proton beams.

Field of Study: Medical Physics

Student's Signature

Academic Year: 2021

Advisor's Signature

ACKNOWLEDGEMENTS

First and foremost, I would like to express my very great appreciation to my advisor Sornjarod Oonsiri, and my co-advisors, Miss Sirinya Ruangchan and Mrs. Puntiwat Oonsiri, Division of Radiation Oncology, Department of Radiology, King Chulalongkorn Memorial Hospital, for allowing me to do research and continued support, guidance, and invaluable advice throughout the process in completing this research.

I would like to thank Associate Professor Sivalee Suriyapee, Division of Radiation Oncology, Department of Radiology, Faculty of Medicine, Chulalongkorn University, for her instruction, support, and insightful comments.

I would like to extend my sincere gratitude to all the medical physicists from the Division of Radiation Oncology, Department of Radiology, King Chulalongkorn Memorial Hospital, for their kind support, valuable comments, and shareable knowledge through this entire process.

I would like to thank Associate Professor Anchali Krisanachinda, Division of Nuclear Medicine, Department of Radiology, Faculty of Medicine, Chulalongkorn University, all lecturers and staff in the Medical Physics Program, Faculty of Medicine, Chulalongkorn University, for their teaching and suggestion.

I would like to thank all Varian engineers from Her Royal Highness Princess Maha Chakri Sirindhorn Proton Center, Division of Radiation Oncology, Department of Radiology, King Chulalongkorn Memorial Hospital, for their time and energy through the experiment.

I would like to thank my classmate from MPCU 18 for their support and kindness. Last but not least, I would like to thank my parents and my close friends for their love, caring, encouragement, understanding, and continuing support to complete this research.

Phatthraporn Thasasi

TABLE OF CONTENTS

	Page
.....	iii
ABSTRACT (THAI)	iii
.....	iv
ABSTRACT (ENGLISH)	iv
ACKNOWLEDGEMENTS	v
TABLE OF CONTENTS	vi
LIST OF TABLES	ix
LIST OF FIGURES.....	x
LIST OF ABBREVIATIONS	1
CHAPTER 1 INTRODUCTION	3
1.1 Background and Rationale.....	3
1.2 Research Objective	5
CHAPTER 2 REVIEW OF RELATED LITERATURE	6
2.1 Theory.....	6
2.1.1 Interactions of the proton with matter	6
2.1.1.1. Inelastic coulomb scattering with atomic electrons	6
2.1.1.2. Elastic coulomb scattering with the nucleus.....	6
2.1.1.3. Non-elastic nuclear interactions.....	6
2.1.2 The physical characteristics of the proton.....	7
2.1.3 The dose distribution of a proton pencil beam in water.....	7
2.1.3.1 Core	7

2.1.3.2 Halo	8
2.1.3.3 Aura	8
2.1.3.4 Spray	8
2.1.4 Integral depth-dose measurement	8
2.1.5 Proton therapy system.....	9
2.1.6 Dose delivery techniques of the proton	10
2.1.6.1 Passive scattering.....	10
2.1.6.2 Active scanning.....	10
2.2 Related literature	11
CHAPTER 3 RESEARCH METHODOLOGY.....	14
3.1 Research Design.....	14
3.2 Research Question	14
3.3 Research Design Model.....	15
3.4 Conceptual Framework.....	16
3.5 Materials	16
3.6 Methods.....	21
3.7 Outcome Measurements.....	24
3.8 Statistical Analysis	24
3.9 Expected Benefit	24
3.10 Ethical Consideration	24
CHAPTER 4 RESULTS	26
4.1 Characteristics of the detectors.....	26
4.1.1 Short-term reproducibility.....	26
4.1.2 Linearity.....	27

4.1.3 Repetition rate dependence.....	28
4.2 Bragg peak range (R_{80}).....	30
4.3 The integral depth-dose curves.....	30
4.4 The geometrical collection efficiency.....	33
CHAPTER 5 DISCUSSION AND CONCLUSION	36
5.1 Discussion	36
5.2 Conclusion	37
REFERENCES.....	38
VITA	41



LIST OF TABLES

	Page
Table 4.1 Short-term reproducibility of all chambers.....	26
Table 4.2 The linearity response of PTW Bragg peak chamber type 34070, Bragg peak chamber type 34089, and PeakFinder.....	27
Table 4.3 The linearity response of IBA Giraffe.....	27
Table 4.4 Repetition rate dependence of PTW Bragg peak chamber type 34070.....	28
Table 4.5 Repetition rate dependence of PTW Bragg peak chamber type 34089.....	29
Table 4.6 Repetition rate dependence of PTW PeakFinder.....	29
Table 4.7 Repetition rate dependence of IBA Giraffe.....	29
Table 4.8 Bragg peak range comparison between measured and NIST.....	30
Table 4.9 Geometrical collection efficiency (%) of 130, 150, 190, and 220 MeV.....	35

LIST OF FIGURES

	Page
Figure 1.1 The integral depth-dose curve.....	4
Figure 2.1 Interactions of the proton with matter.....	6
Figure 2.2 The physical characteristics of the proton.....	7
Figure 2.3 The dose distribution of a proton pencil beam in water.....	8
Figure 2.4 The chamber setup for the integral depth-dose measurement.	9
Figure 2.5 Proton therapy system.....	10
Figure 2.6 Dose delivery techniques of the proton.....	11
Figure 3.1 Research Design Model.....	15
Figure 3.2 Conceptual Framework.....	16
Figure 3.3 The Varian ProBeam™ Compact spot scanning system.....	17
Figure 3.4 PTW MP3-PL water phantom.....	18
Figure 3.5 Solid water phantom.....	18
Figure 3.6 Detectors.....	20
Figure 3.7 PTW Bragg peak chamber setup for measuring characteristics.....	21
Figure 3.8 The chambers setup for integral depth dose measurements.....	22
Figure 3.9 Bragg peak range (R_{80}).....	23
Figure 3.10 The certificate of approval from the Institutional Review Board (IRB).....	25
Figure 4.1 The linearity response: (a) PTW Bragg peak chamber type 34070, (b) PTW Bragg peak chamber type 34089, (c) PTW PeakFinder, and (d) IBA Giraffe.....	28
Figure 4.2 The integral depth dose curves acquired with all chambers for proton beam energies of 70, 100, 130, 150, 190, and 220 MeV.	31
Figure 4.3 The curve arrangements of all chambers in the largest deviation region. ...	32

Figure 4.4 The integral depth dose curves acquired with all chambers of 220 MeV...33	
Figure 4.5 The ratios of depth-dose curves acquired with two types of PTW Bragg peak chamber 34070 and 34089.34	34
Figure 4.6 The ratios of depth-dose curves acquired with PTW PeakFinder and Bragg peak chamber 34089.34	34
Figure 4.7 The ratios of depth-dose curves acquired with IBA Giraffe and PTW Bragg peak chamber 34089.35	35



LIST OF ABBREVIATIONS

Abbreviation terms

BP8	PTW Bragg peak chamber type 34070
BP15	PTW Bragg peak chamber type 34089
CFRP	Carbon fiber reinforced polymer
cm	Centimeter
CSDA	Continuous slowing down approximation
d	Diameter
E	Energy
IC	Ionization chamber
IC ₈	Ionization chamber with 8 cm diameter
IC ₁₂	Ionization chamber with 12 cm diameter
IC ₄₀	Ionization chamber with 40 cm diameter
IC _d	Ionization chamber with d cm diameter
IDD	Integral depth-dose curve
IDD _d	Integral depth-dose curve of ionization chamber with d cm diameter
IDD ₁₅	Integral depth-dose curve of ionization chamber with 15 cm diameter
IMPT	Intensity-modulated proton therapy
MC	Monte Carlo
MLIC	Multi-layer ionization chamber
mm	Millimeter
MU	Monitor unit
MeV	Mega electron volt
nC	Nanocoulomb
NIST	National Institute of Standards and Technology
PMMA	Polymethyl Methacrylate

R_{80}	The depth of the distal 80% of the maximum dose
SOBP	Spread-out Bragg Peak
TPS	Treatment planning system
WET	Water-equivalent thickness
μm	Micrometer



CHAPTER 1

INTRODUCTION

1.1 Background and Rationale

Over the last decade, proton therapy with pencil beam scanning techniques, implemented in many proton facilities, gained more importance in radiation oncology. Compared to conventional treatments (photons), protons can potentially decrease side effects and increase tumor control probability. Besides the physical characteristics of the proton (1), there are relatively low entrance dose, maximum dose or Bragg peak at the target, and rapid dose fall-off beyond the peak to spare normal tissues. These properties provide superior sparing of normal tissues, reduce radiation side effects, and secondary cancer in a pediatric patient.

The Varian ProBeam™ Compact (Varian Medical System, Palo Alto, CA, USA) system composes the cyclotron with maximum energy up to 220 MeV. It offers treatment functionality with the gantry rotation. One of the main tasks for beam commissioning is preparing the treatment planning systems for clinical use. The proton spot characteristics have to be considered in dose calculation algorithms for clinical treatment planning systems, directly impacting the treatment quality. The input data needed for the proton dose model in the treatment planning systems are the integral depth-dose curves, absolute dose calibration, and spot profiles in the air (2). This research focuses on the integral depth-dose curve because it is an essential factor that has to be determined and introduced into the proton treatment planning system before clinical use and it also represents beam quality and physical characteristics of the proton beam.

As shown in figure 1.1, the integral depth-dose curve is the total dose on an infinite plane normal to the beam's central axis along the depths (3). The proton pencil beam's initial size is a few millimeters, but the beam gets broadened due to a halo. A halo is the deposited dose around the primary beam and mainly produced by large scattered secondary protons. It results from nuclear and coulomb interactions of the primary proton beam in the medium such as nozzle and

detection medium (e.g., water). The contribution from secondary protons or a halo is most pronounced at intermediate depths and the highest energy proton beam (4-7).

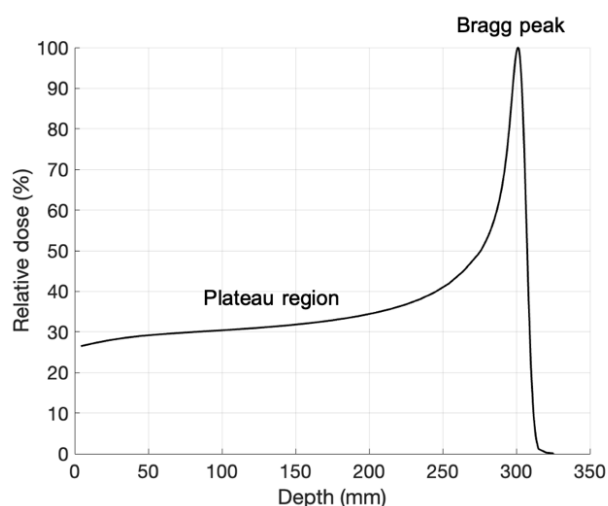


Figure 1.1 The integral depth-dose curve.

Static, monoenergetic pencil beams should be delivered for the integral depth-dose curve measurements. The integral depth-dose curve should be measured with a large-diameter plane-parallel ionization chamber to acquire the entire pencil beam due to halo or low dose surrounding the primary beam. There is a missing dose deposited outside the active area of the chamber. In order to measure the integral depth-dose curve, the PTW Bragg peak chamber type 34070 with 8 cm diameter is the most frequently used in clinical proton centers. However, it was indicated by Langner UW et al. (2) and Baumer C et al. (4) that for higher energies, PTW Bragg peak chamber type 34070 was not large enough to acquire all the secondary protons from the proton pencil beam. Moreover, Baumer C et al. found that the IBA Stingray chamber with 12 cm diameter requires 2% and 3.5% less correction than the PTW Bragg peak chamber type 34070 for 180 and 226.7 MeV, respectively.

Currently, there are many commercially available large-diameter ionization chambers, such as PTW PeakFinder with 8 cm diameter, IBA Stingray chamber with 12 cm diameter, IBA Giraffe with 12 cm diameter, and PTW Bragg peak chamber type 34089 with 15 cm diameter. Consequently, this research aims to determine

the integral depth-dose curves and assess the geometrical collection efficiency at intermediate depths of four different detectors with diameters of 8, 12, and 15 cm in proton pencil beam scanning.

1.2 Research Objective

To determine the differences of integral depth-dose curves and assess the geometrical collection efficiency at intermediate depths of different detector diameters in proton pencil beam scanning



CHAPTER 2

REVIEW OF RELATED LITERATURE

2.1 Theory

2.1.1 Interactions of the proton with matter (1)

2.1.1.1. Inelastic coulomb scattering with atomic electrons

Protons interact with atomic electrons through inelastic coulombic interactions, continuously losing kinetic energy and slowing down, resulting in the finite range of protons in the matter. They travel in an almost straight line because a proton's rest mass is 1832 times greater than an electron. It is shown in figure 2.1(a).

2.1.1.2. Elastic coulomb scattering with the nucleus

A proton passes close to the atomic nucleus through elastic coulombic interaction and deflects from its original straight-line trajectory due to the large mass of the nucleus. It is shown in figure 2.1(b).

2.1.1.3. Non-elastic nuclear interactions

Non-elastic nuclear reactions between protons and the atomic nucleus, as shown in figure 2.1(c), are less frequent but have a much more profound effect in terms of the fate of an individual proton. The proton enters the nucleus, which may emit a proton, deuteron, triton, heavier ion, or one or more neutrons.

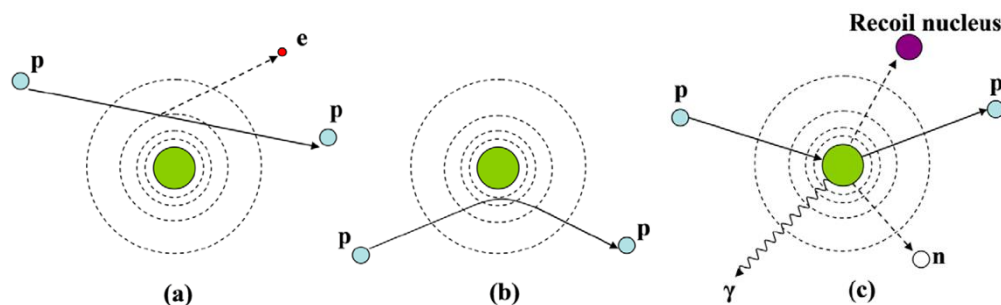


Figure 2.1 Interactions of the proton with matter: (a) Inelastic coulomb scattering with electrons, (b) Elastic coulomb scattering with the nucleus, (c) Non-elastic nuclear interaction (p: proton, e: electron, n: neutron, and γ : gamma rays).

2.1.2 The physical characteristics of the proton

The contribution of proton dose is the most deposited in the tumor while minimal in the entrance and no exit dose (8). Figure 2.2 (9) shows the physical characteristics of the proton that is clinically useful in many cases, relatively low entrance dose or plateau region, maximum dose, or Bragg peak at the tumor, and rapid distal fall-off of dose at the end of the range to spare normal tissues. These properties allow proton beams to treat tumors of various sizes and locations while sparing normal tissue and reducing radiation-induced side effects and secondary cancer (1).

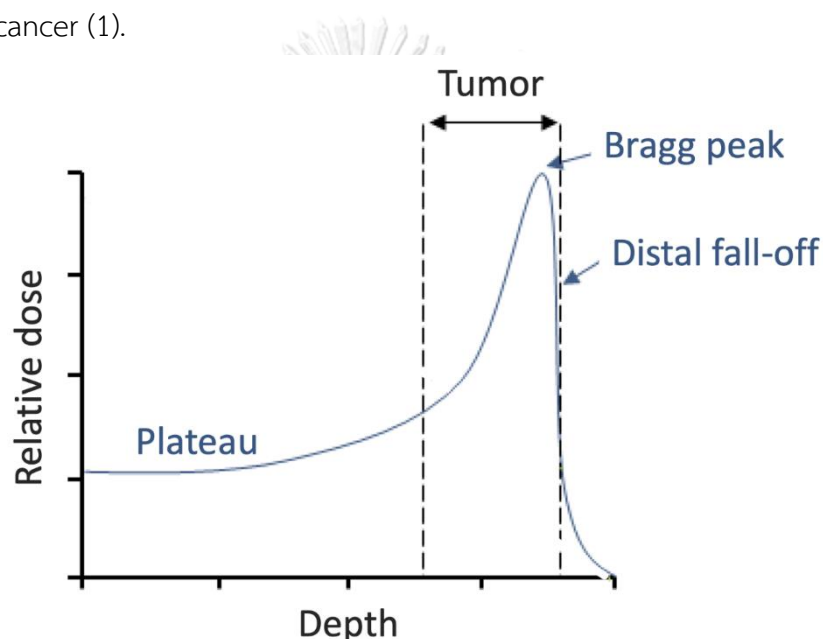


Figure 2.2 The physical characteristics of the proton.

2.1.3 The dose distribution of a proton pencil beam in water (5)

The components of a proton pencil beam's dose distribution in water, as shown in figure 2.3, are caused by basic physics and beam contamination. It consists of a core, a halo, an aura, and (possibly) a spray.

2.1.3.1 Core

Core for the primary beam from primary protons is produced by multiple coulomb scattering and slowed down by multiple collisions with atomic electrons.

2.1.3.2 Halo

Halo for the low dose region of deposited dose around the primary beam is mainly produced by large scattered secondary protons from elastic interactions with hydrogen, elastic, and inelastic interactions with oxygen, and non-elastic interactions with oxygen. The halo radius is approximately one-third of the beam range. It is most pronounced at intermediate depths of the incident beam and the highest energy (4-7).

2.1.3.3 Aura

Aura is neutral secondary including neutrons and gamma rays from inelastic and non-elastic nuclear interactions. It is very large, pervading the patient, treatment room, shielding, and depositing unwanted doses. Its behavior at large distances is influenced by the materials traversed, such as shielding.

2.1.3.4 Spray

Spray for beam contamination is in principle avoidable. It comes from components in the beamline such as profile monitors, beam pipes, or degraders near the patient.

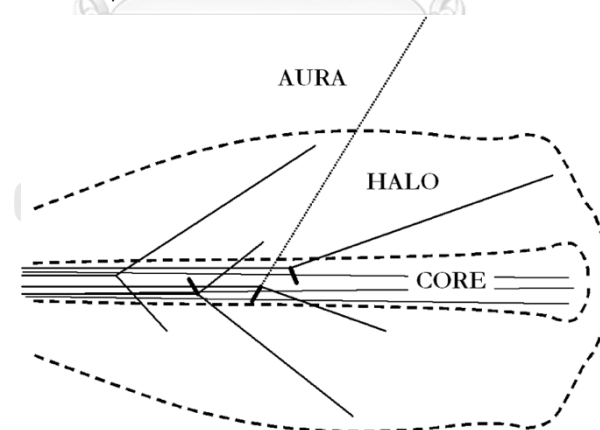


Figure 2.3 The dose distribution of a proton pencil beam in water.

2.1.4 Integral depth-dose measurement

For the Integral depth-dose measurement, static, monoenergetic pencil beams should be delivered and acquired with a large-diameter plane-parallel ionization chamber to collect the dose deposited by both primary and secondary

particles. Nowadays, commercially available large-diameter ionization chambers have a diameter of 8–15 cm. The chamber is placed in a water phantom, as shown in figure 2.4, and moved along the beam axis to acquire the entire Bragg peak curve (7). A water phantom with sub-millimetric positioning accuracy and a fixed source-to-surface distance should be used. The depth measurement points can be a non-uniform spacing. However, the measurement step size should be less than 1 mm to determine the Bragg peak adequately (3).

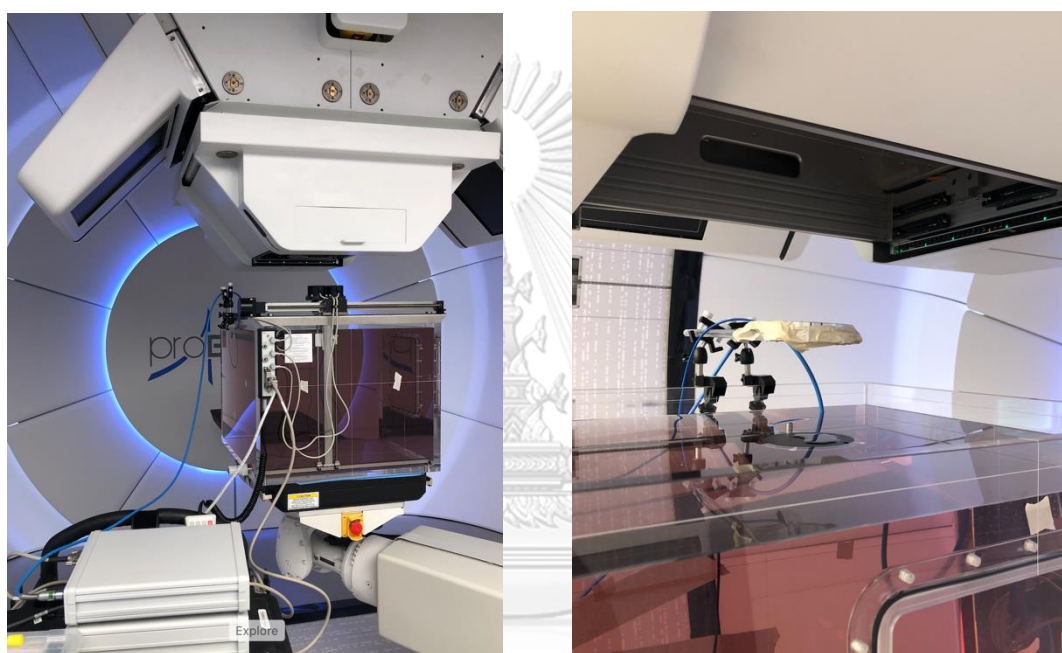


Figure 2.4 The chamber setup for the integral depth-dose measurement.

2.1.5 Proton therapy system (10)

The proton therapy system, as shown in figure 2.5, uses a superconducting cyclotron with a hydrogen source to accelerate the proton to the maximum energy at the exit of the cyclotron. Once the protons have been accelerated, the energy selection system degrades the beam to produce various lower energies. Currently, approximately 40 cm depth with 250 MeV can be treated with a degrader, allowing for the treatment of shallower depths. After leaving the energy selection system, the proton beam travels in a vacuum within the beamline. It is guided by various magnets, including dipole and quadrupole magnets, which can deflect and focus

the beam. These magnets can be precisely controlled to focus various energy beams. The gantry can be rotated 360 degrees around a patient. Nozzles are part of the beam delivery system and contain multiple components. The two main types of proton delivery systems are passive scattering and active scanning.

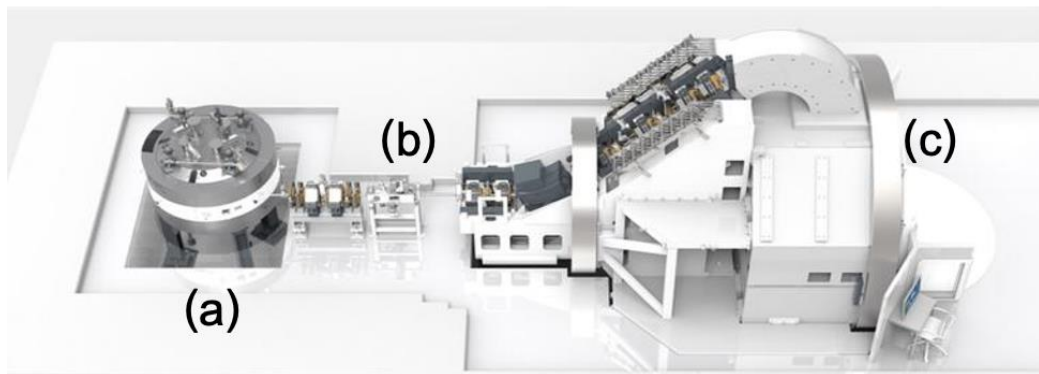


Figure 2.5 Proton therapy system: (a) Cyclotron, (b) Beamline, and (c) Gantry.

2.1.6 Dose delivery techniques of the proton

Proton therapy is a type of radiation therapy that uses high proton energy to treat cancer. Dose delivery techniques are divided into two types based on nozzle components: passive scattering and active scanning. Active scanning is increasingly used in many proton centers because it provides dose escalation and more target dose conformity than other treatment techniques.

2.1.6.1 Passive scattering

Passive scattering, as shown in figure 2.6(a) (11), is a simple and traditional technique that uses a modulator to spread-out Bragg peak (SOBP) over a volume in-depth and scatter foils to expand the narrow beam into a wide beam for covering the target. The proton beam can be shaped laterally and distally using a collimator and compensator.

2.1.6.2 Active scanning

The active scanning or pencil beam scanning, as shown in figure 2.6(b) (11), is a narrow proton beam with variable intensity and energy that is magnetically steered across the target. The diameter and range of the pencil

beam vary depending on energy. The shape of the spots is also a function of the beam steering in the system. In addition, this technique allows for conformal dose without using both collimators and compensators, which are neutron dose sources to the patient (12).

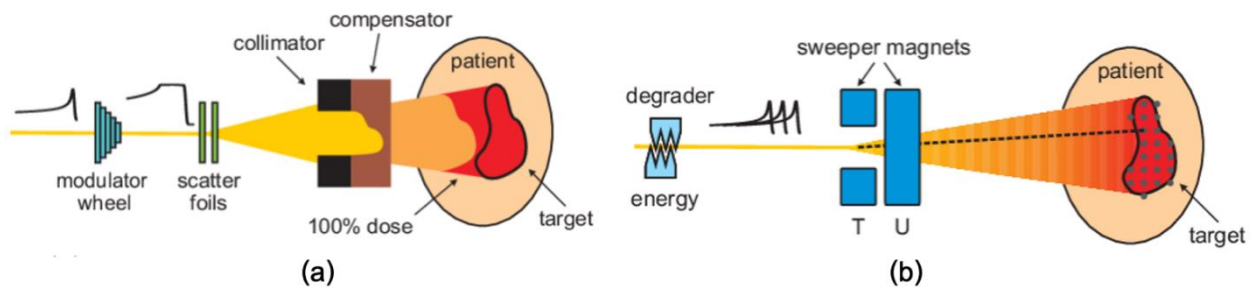


Figure 2.6 Dose delivery techniques of the proton: (a) Passive scattering and (b) Pencil beam scanning.

2.2 Related literature

Langner UW et al. (2) compared commissioning beam data of proton pencil beams for the first two Varian ProBeam™ sites in the United States. There are many parts of beam commissioning whose study relates to the integral depth dose curves. They acquired an integral depth-dose curve using a PTW Bragg peak chamber with 8 cm diameter and an IBA Stingray chamber with 12 cm diameter in a water phantom. The Bragg peak ranges (R_{80}) were measured and compared to the theoretical calculation using the Bortfeld equation ($R_{80} = 0.00244 * E^{1.75}$). The results showed that R_{80} differences between the measured and theoretical values were within tolerance. However, they found that in the shoulder region of higher energies, the integral depth-dose curve of the IBA Stingray chamber is higher than the PTW Bragg peak chamber. Therefore, they suggest that an 8 cm diameter chamber is not large enough to acquire all secondary protons or halo and this agrees with the halo effect data from Monte Carlo studies.

Baumer C et al. (4) evaluated the improvement in the geometrical collection efficiency of the IBA Stingray chamber with 12 cm diameter over the PTW Bragg peak chamber. They acquired an integral depth-dose curve using the IBA Stingray chamber and PTW Bragg peak chamber and then compared it to IBA PPC05, which was acquired under broad field conditions. The proportion of an integral depth-dose curve acquired with two different chamber diameters was calculated to assess the relative collection efficiency. They found that the transition zone between the entrance plateau and the proximal rise of the Bragg peak has the largest deviations between the curves. The highest integral depth-dose curve is from IBA PPC05 followed by the IBA Stingray chamber and PTW Bragg peak chamber. Therefore, the IBA Stingray chamber has increased geometrical collection efficiency up to 2.0% and 3.5% for intermediate and high energies at intermediate depth, compared to the PTW Bragg peak chamber with an 8 cm diameter which refers to the halo's scenario mainly produced in the detection medium. They also evaluated if a large electrode multi-layer ionization chamber (IBA Giraffe) could replace the combination of a chamber and water phantom. They compared the integral depth-dose curves measured with the IBA Giraffe to the IBA Stingray of the same diameter. They found that the Bragg peak of an IBA Giraffe acquisition is a bit flatter than IBA Stingray. Therefore, the large electrode multi-layer ionization chamber allows fast quality assurance of the integral depth-dose curve. However, they said that the users should be careful of small distortions in the Bragg peak and not be used as input data for the proton treatment planning system.

Mojzeszek N et al. (13) investigated the geometrical collection efficiency of a plane-parallel ionization chamber with the chamber diameter and energy. They derived the integral depth-dose curve directly from the Monte Carlo calculations. The geometrical efficiency (ϵ_g) for the ionization chamber's diameter (d) from 4 to 40 cm was calculated by this equation ($\epsilon_g(z) = \text{IDD}_d(z)/\text{IDD}_{40}(z)$). The signal of each IC_d was compared with IC_{40} because it can collect the entire proton pencil beam. They calculated the geometrical efficiency of ionization chambers with different diameters

from 4 to 40 cm in four different depths (0, 2, 16, and 31.6 cm) at 226.08 MeV. They found that the geometrical efficiency of IC₈ and IC₁₂ at a depth of 16 cm was 0.942 and 0.964, respectively. For lower energies, these values will be higher as reducing of missing dose. They also calculated ϵ_g of IC₈ and IC₁₂ for proton energy from 70 to 226.08 MeV at the mid-range depth. They found that the geometrical efficiency of IC₈ and IC₁₂ is higher than 0.99 for energies less than 160 and 190 MeV, respectively. It means that IC₈ and IC₁₂ are enough for integral depth-dose curve measurements without additional corrections in the energy range mentioned above. As a result, they show that the currently available large-sized ionization chamber could be used with better than 0.99 geometrical efficiencies up to 160 MeV (for IC₈, i.e. d = 8 cm) and 190 MeV (for IC₁₂, i.e. d = 12 cm) without any specific corrections.



CHAPTER 3

RESEARCH METHODOLOGY

3.1 Research Design

This research is an observational descriptive study.

3.2 Research Question

What are the differences of integral depth-dose curves and the geometrical collection efficiency at intermediate depths of different detector diameters in proton pencil beam scanning?



3.3 Research Design Model

This research is divided into four main parts, characteristics of the detectors, Bragg peak range (R_{80}), the integral depth-dose curves, and the geometrical collection efficiency. The details of the research design model are presented in figure 3.1.

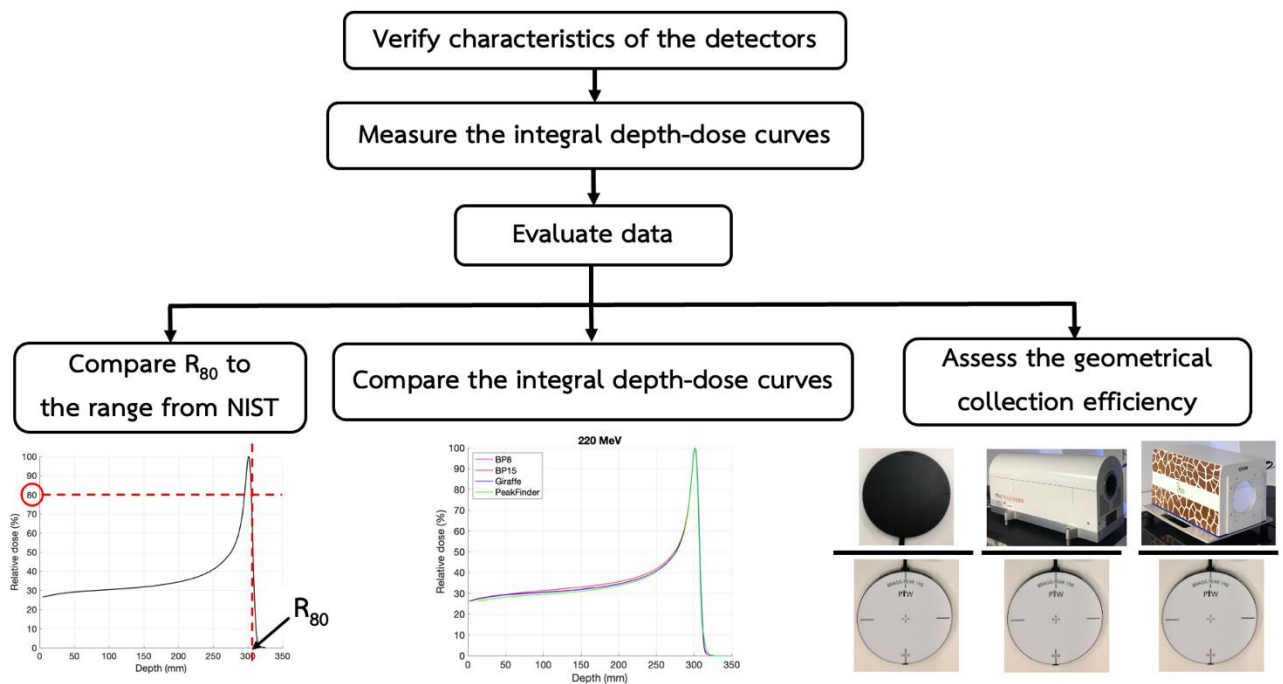


Figure 3.1 Research Design Model.

3.4 Conceptual Framework

The integral depth-dose curve is influenced by factors such as machine, energy, detector diameter, and the detection medium are presented in figure 3.2.

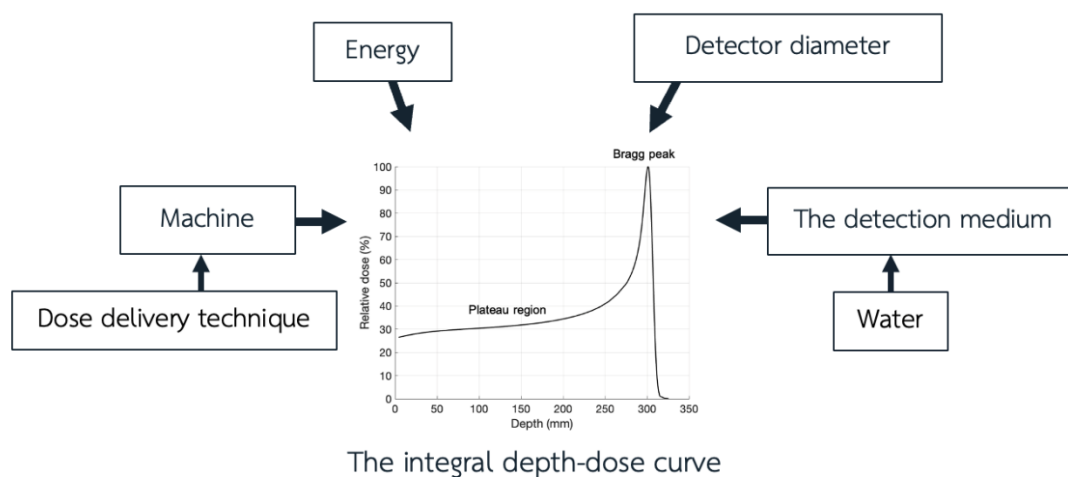


Figure 3.2 Conceptual Framework.

3.5 Materials

3.5.1 Proton therapy system (2) มหาวิทยาลัย

The Varian ProBeam™ Compact spot scanning system (Varian Medical System, Palo Alto, CA, USA) from Varian Medical Systems offers the latest techniques in intensity-modulated proton therapy (IMPT). The Varian ProBeam™ Compact system exclusively uses spot scanning gantries that dynamically scan the beam from one spot to another and uses a superconducting cyclotron that allows proton acceleration from 70 to 220 MeV by an energy selection system. The Varian ProBeam™ Compact spot scanning system is shown in figure 3.3.



Figure 3.3 The Varian ProBeam™ Compact spot scanning system.

3.5.2 PTW MP3-PL water phantom (14)

The MP3-PL water phantom (PTW, Freiburg, Germany) is a 3D phantom for remote-controlled scans with 100 μm increments to acquire the Bragg peak region. The scanning range is 50 cm horizontally and 40.5 cm vertically. A thin exchangeable entrance window of Polymethyl Methacrylate (PMMA) makes the system suitable for horizontal beamline measurements. Dual-chamber holders allow the fixation of Bragg peak chambers to the water phantom. For the integral depth-dose measurements, the reference chamber is mounted to the outside of the water phantom and the measuring chamber is mounted to the moving mechanism. MEPHYSTO mc^2 software and TBA electronics are used to operate the water phantom system. The PTW MP3-PL water phantom is shown in figure 3.4.

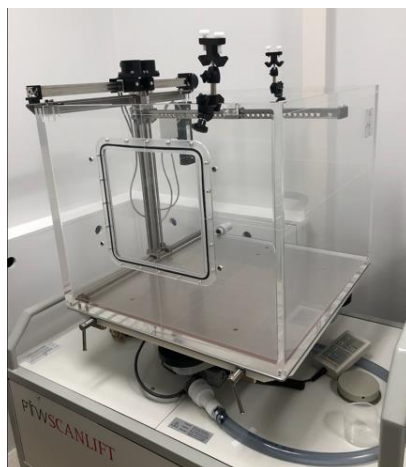


Figure 3.4 PTW MP3-PL water phantom.

3.5.3 Solid Water Phantom

The solid water phantoms (RMI-Gammex, Inc., Middleton, WI, USA) with a density of 1.02 g/cm^3 and an atomic number of 5.95 are made in square slabs of $30 \times 30 \text{ cm}^2$ with various thicknesses as shown in figure 3.5.



Figure 3.5 Solid water phantom.

3.5.4 Detectors

3.5.4.1 PTW Bragg peak chamber type 34070 (BP8)

The Bragg peak chamber type 34070 (PTW, Freiburg, Germany) is a standard chamber for integral depth-dose curve acquisition. The electrode diameter is 8 cm with an electrode spacing of 2 mm, and the sensitive volume is 10.5 cm^3 . According to the vendor, the entrance window is

3.35 mm of PMMA, corresponding to a water-equivalent thickness for proton beams of 4.0 mm. The chamber is mounted in an MP3-PL water phantom to acquire the integral depth-dose curves. The PTW Bragg peak chamber type 34070 is shown in figure 3.6(a).

3.5.4.2 PTW Bragg peak chamber type 34089 (BP15)

The Bragg peak chamber type 34089 (PTW, Freiburg, Germany) is the latest and largest designed plane-parallel ionization chamber, with a 15 cm electrode diameter and 2 mm electrode spacing. The sensitive volume is 34 cm³. According to the vendor, the entrance window is 2.47 mm of carbon fiber reinforced polymer (CFRP), which corresponds to a water-equivalent thickness for proton beams of 4.65 mm. This chamber is mounted in an MP3-PL water phantom, the same as PTW Bragg peak chamber type 34070. The PTW Bragg peak chamber type 34089 is shown in figure 3.6(b).

3.5.4.3 PTW PeakFinder

The PeakFinder (PTW, Freiburg, Germany) is a closed water column containing approximately 6 liters of distilled water with anti-corrosion fluid and designed especially for the highest precision peak detection with a spatial resolution of 10 μ m. The signals of the built-in thin window Bragg peak chamber type 34080, the same type as thick window Bragg peak chamber type 34070, are read out by the TANDEM XDR electrometer. The PTW PeakFinder is shown in figure 3.6(c).

3.5.4.4 IBA Giraffe

The Giraffe (IBA dosimetry, Schwarzenbruck, Germany) is a large electrode multi-layer ionization chamber (MLIC) designed to measure the longitudinal depth-dose distribution of central-axis proton pencil beams, which is composed of 180 plane-parallel ionization chambers fabricated with printed circuit board technologies. The outer graphite layers of each printed circuit board plate form the circular electrodes with a diameter of 12 cm and a detector spacing of 2 mm. The air gap between the two plates is approximately 1 mm. The water-equivalent thickness of each channel is set to a value between 1.85 mm and 1.90 mm by the vendor. The effective

points of measurements range from about 2 mm to 330 mm in a depth axis. A uniformity calibration should be performed before the operation of the multi-layer ionization chamber to correct the relative dose of each channel to match the reference measurement in water (4, 15). The IBA Giraffe is shown in figure 3.6(d).

In this research, a uniformity calibration was performed at 220 MeV by PTW Bragg peak chamber type 34070.

3.5.4.5 PTW x-ray therapy monitor chamber type 7862

The x-ray therapy monitor chamber type 7862 (PTW, Freiburg, Germany) is used as a reference chamber with a diameter of 9.65 cm and a physical window thickness of 0.2 mm (2). The PTW x-ray therapy monitor chamber type 7862 is shown in figure 3.6(e).

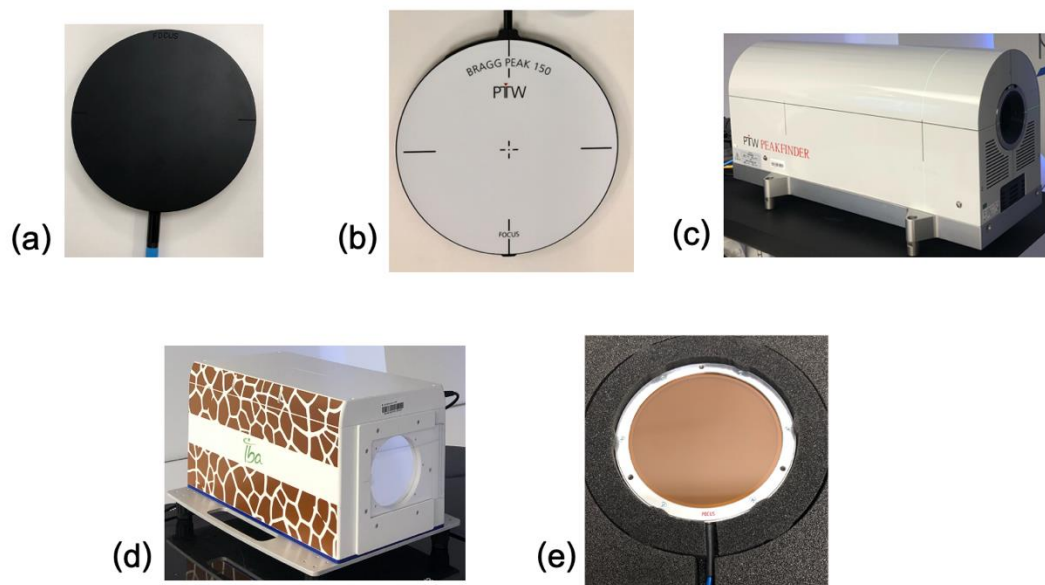


Figure 3.6 Detectors: (a) PTW Bragg peak chamber type 34070, (b) PTW Bragg peak chamber type 34089, (c) PTW PeakFinder, (d) IBA Giraffe, and (e) PTW x-ray therapy monitor chamber type 7862.

3.6 Methods

1. Characteristics of the detectors

All parts of characteristics of the detectors were undertaken on 150 MeV proton beams from the Varian ProBeam™ Compact spot scanning system in a solid water phantom before measuring the integral depth-dose curves. The experimental setup of the PTW Bragg peak chamber is shown in figure 3.7.

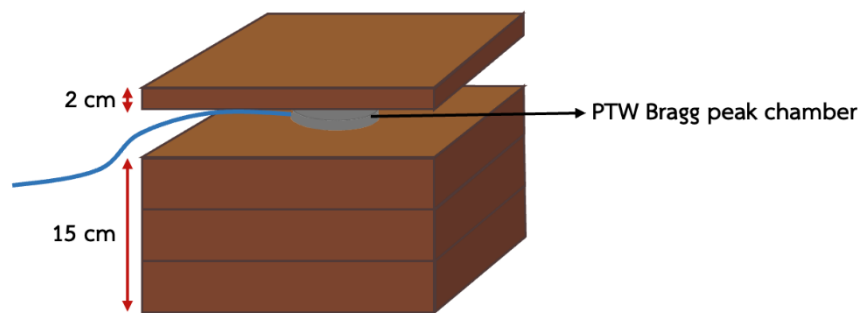


Figure 3.7 PTW Bragg peak chamber setup for measuring characteristics.

1.1 Short-term reproducibility

The IBA Giraffe was irradiated for 100 MU and the other chambers were irradiated for 10,000 MU repeatedly ten times.

1.2 Linearity

The linearity was measured for MU settings ranging from 10 to 1,000 MU and 500 to 50,000 MU with IBA giraffe and the other chambers, respectively.

1.3 Repetition rate dependence

The fixed 100 and 10,000 MU were delivered to IBA Giraffe and the other chambers, respectively with different dose rates (50,000, 100,000, 750,000, 1,500,000, 3,000,000 MU/min). Values were normalized to 750,000 MU/min for all chambers.

2. Measurement of the integral depth-dose curves

Static and monoenergetic pencil beams with proton energies of 70, 100, 130, 150, 190, and 220 MeV were delivered to measure the integral depth dose curves using two types of PTW Bragg peak chamber: 34070 and 34089 mounted in MP3-PL water phantom for vertical beamline, and PTW PeakFinder and IBA Giraffe for horizontal beamline.

For the PTW Bragg peak chamber and PTW PeakFinder, The step size was divided into three parts: 3 mm for 70 and 100 MeV, 5 mm for 130 and 150 MeV, and 10 mm for 190 and 220 MeV (the plateau region), 0.5 mm (the peak region), and 5 mm (the distal fall-off region). The measured integral depth-dose curves were corrected for the WETs of the reference chamber and the entrance window of the chamber. The setup of four chambers for integral depth dose measurements is shown in figure 3.8.

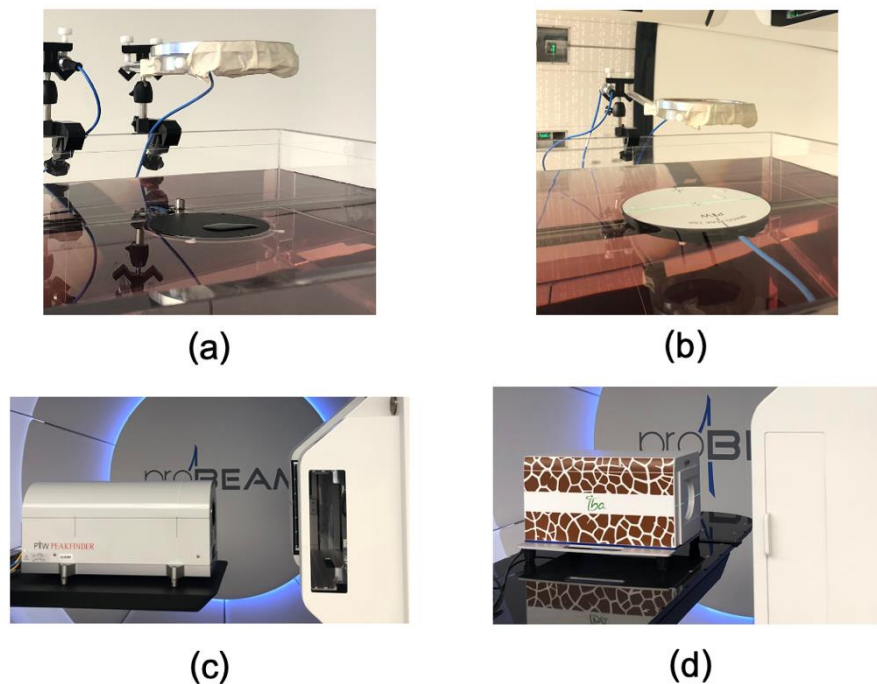


Figure 3.8 The chambers setup for integral depth dose measurements: (a) PTW Bragg peak chamber type 34070, (b) PTW Bragg peak chamber type 34089, (c) PTW PeakFinder, and (d) IBA Giraffe.

3. Comparison of Bragg peak range (R_{80}) (tolerance: 1 mm)

Bragg peak range (R_{80}) was measured three times and compared the mean of R_{80} to ranges from the National Institute of Standards and Technology (NIST) (16) obtained from Monte Carlo calculations by assuming continuous slowing down approximation (CSDA) without considering multiple coulomb scattering and nuclear interaction to validate setup positions, beam energies, and WETs of the entrance window of the chambers according to the vendor. Bragg peak range (R_{80}) is shown in figure 3.9.

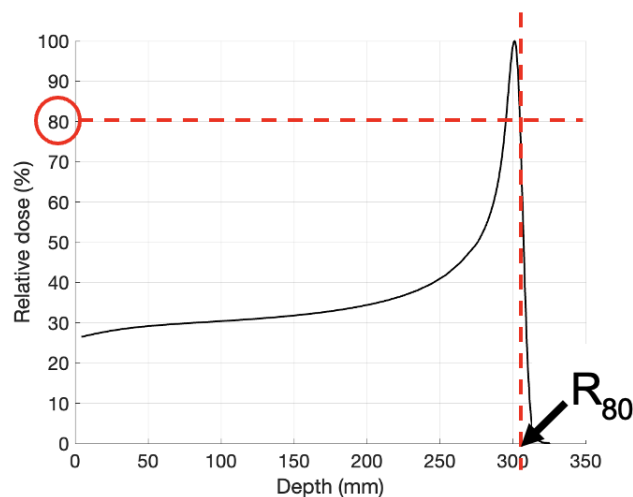


Figure 3.9 Bragg peak range (R_{80}).

4. Comparison of the integral depth-dose curves

All integral depth-dose curves were scaled to a maximum of 100% of the dose and shifted in depth to match R_{80} from NIST to eliminate the range uncertainty before comparing the integral depth-dose curves measured with PTW Bragg peak chamber type 34070, PTW Bragg peak chamber type 34089, PTW PeakFinder, and IBA Giraffe.

5. Assessment of the geometrical collection efficiency

The geometrical collection efficiency of detectors was calculated at half of R_{80} (the intermediate depth) by comparing PTW Bragg peak chamber type 34070,

PTW PeakFinder, and IBA Giraffe to PTW Bragg peak chamber type 34089 as the following equation, where d represents the chamber diameter in 8 and 12 cm.

$$\text{The geometrical collection efficiency (\%)} = \left(1 - \frac{\text{IDD}_d(z)}{\text{IDD}_{15}(z)}\right) \times 100 \quad (1)$$

3.7 Outcome Measurements

1. **Independent variables:** Detector diameter and energy
2. **Dependent variables:** The integral depth-dose curve, Bragg peak range (R_{80}), and the geometrical collection efficiency

3.8 Statistical Analysis

The data of characteristics of the detectors were presented as the mean, the standard deviation (SD), and the coefficient of variation (%CV). The data of Bragg peak ranges (R_{80}) were presented as maximum deviation and difference between NIST and measured values.

3.9 Expected Benefit

The geometrical collection efficiency at intermediate depths in a large-diameter plane-parallel ionization chamber for proton pencil beam scanning will be improved.

3.10 Ethical Consideration

This study required the dosimetric data of the integral depth-dose curves from the Division of Radiation Oncology, Department of Radiology, King Chulalongkorn Memorial Hospital. Therefore, this research was submitted for ethical consideration and was approved by the Institutional Review Board (IRB), Faculty of

Medicine, Chulalongkorn University (IRB 504/64). The certificate is shown in figure 3.10.

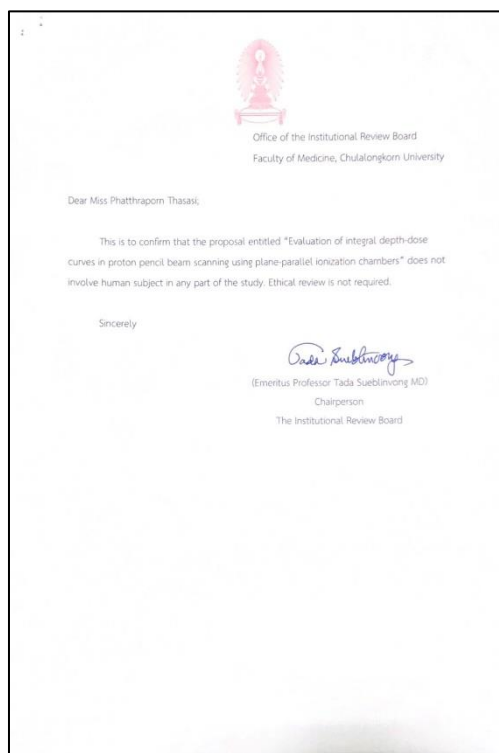


Figure 3.10 The certificate of approval from the Institutional Review Board (IRB), Faculty of Medicine, Chulalongkorn University.

จุฬาลงกรณ์มหาวิทยาลัย
CHULALONGKORN UNIVERSITY

CHAPTER 4

RESULTS

4.1 Characteristics of the detectors

4.1.1 Short-term reproducibility

The coefficient of variation was less than 0.2% for all chambers, with a minimum of 0.04% for two types of PTW Bragg peak chamber, indicating good short-term reproducibility as shown in table 4.1.

Table 4.1 Short-term reproducibility of all chambers

No.	Signal (nC)			
	BP8	BP15	PeakFinder	Giraffe
1	215.9	196.4	187.2	1.033
2	215.9	196.4	187.0	1.034
3	215.9	196.3	187.0	1.034
4	215.7	196.2	186.7	1.031
5	215.8	196.4	186.6	1.032
6	216.0	196.3	186.8	1.033
7	215.9	196.4	186.8	1.033
8	215.8	196.3	186.5	1.032
9	215.9	196.5	186.7	1.032
10	216.0	196.4	186.8	1.031
Mean ± SD	215.88 ± 0.09	196.36 ± 0.08	186.81 ± 0.21	1.033 ± 0.001
%CV	0.04	0.04	0.11	0.09

4.1.2 Linearity

In terms of MU linearity, the response of all chambers was linear to the MU setting as shown in tables 4.2 and 4.3. Values of $R^2 > 0.99$ with the linear function were found for all chambers as shown in figure 4.1.

Table 4.2 The linearity response of PTW Bragg peak chamber type 34070, Bragg peak chamber type 34089, and PeakFinder

MU	Signal (nC)		
	BP8	BP15	PeakFinder
500	10.8	9.8	9.3
1000	21.6	19.6	18.7
2000	43.2	39.3	37.3
5000	108.0	98.2	93.1
10000	216.0	196.5	186.1
20000	432.1	393.0	372.3
50000	1080.0	982.2	930.5

Table 4.3 The linearity response of IBA Giraffe

MU	Signal (count)
	Giraffe
10	513.5
20	1033.4
50	2579.4
100	5155.2
300	15472.6
500	25816.6
1000	51625.2

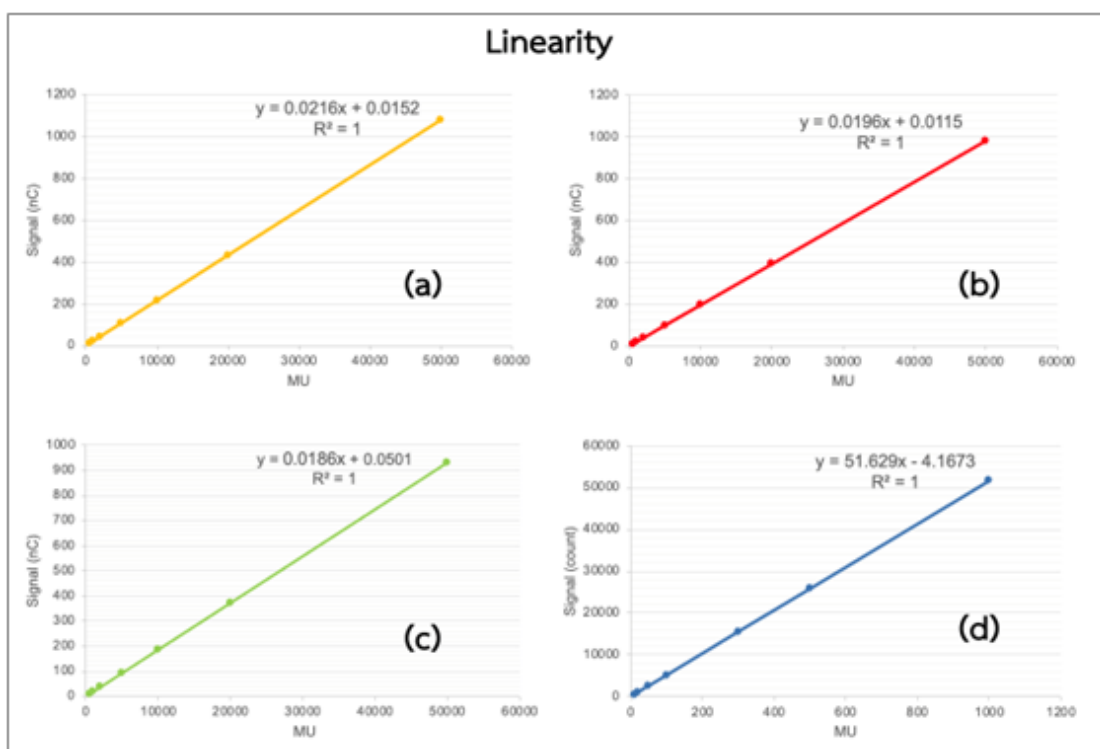


Figure 4.1 The linearity response: (a) PTW Bragg peak chamber type 34070, (b) PTW Bragg peak chamber type 34089, (c) PTW PeakFinder, and (d) IBA Giraffe.

4.1.3 Repetition rate dependence

Repetition rate dependence was within 0.3% for all chambers as shown in table 4.4 to 4.7.

Table 4.4 Repetition rate dependence of PTW Bragg peak chamber type 34070

Repetition rate (MU/min)	Signal (nC)				Normalize
	1	2	3	Mean	
50000	216.1	216.0	216.1	216.1	0.999
100000	216.3	216.0	216.1	216.1	1.000
750000	216.1	216.4	216.1	216.2	1.000
1500000	216.2	216.4	216.4	216.3	1.001
3000000	216.3	216.5	216.6	216.5	1.001

Table 4.5 Repetition rate dependence of PTW Bragg peak chamber type 34089

Repetition rate (MU/min)	Signal (nC)				Normalize
	1	2	3	Mean	
50000	196.3	196.3	196.2	196.3	0.998
100000	196.3	196.4	196.4	196.4	0.999
750000	196.6	196.6	196.7	196.6	1.000
1500000	196.5	196.7	196.6	196.6	1.000
3000000	196.5	196.4	196.6	196.5	0.999

Table 4.6 Repetition rate dependence of PTW PeakFinder

Repetition rate (MU/min)	Signal (nC)				Normalize
	1	2	3	Mean	
50000	186.1	186.2	186.1	186.1	0.998
100000	186.0	186.1	186.2	186.1	0.998
750000	186.4	186.6	186.5	186.5	1.000
1500000	186.7	186.7	186.8	186.7	1.001
3000000	186.5	186.6	186.7	186.6	1.001

Table 4.7 Repetition rate dependence of IBA Giraffe

Repetition rate (MU/min)	Signal (count)				Normalize
	1	2	3	Mean	
50000	5161.5	5152.9	5156.1	5156.9	0.998
100000	5152.7	5152.3	5156.2	5153.7	0.997
750000	5169.2	5171.6	5166.6	5169.1	1.000
1500000	5175.7	5169.9	5162.9	5169.5	1.000
3000000	5166.9	5172.2	5161.6	5166.9	1.000

4.2 Bragg peak range (R_{80})

The R_{80} differences between NIST and measured values of all chambers from 70 to 220 MeV are shown in table 4.8. R_{80} differences were found to be within a 1 mm tolerance (17), with a maximum of 0.9 mm for IBA Giraffe at 190 MeV. According to the vendor, it indicates the accuracy of setup positions of all chambers, beam energies, and WETs of the entrance window.

Table 4.8 Bragg peak range comparison between measured and NIST

Energy (MeV)	NIST (mm)	R_{80} measured (mm)				R_{80} difference (mm)			
		BP8	BP15	PeakFinder	Giraffe	BP8	BP15	PeakFinder	Giraffe
70	40.8	40.6	40.6	40.6	41.1	-0.2	-0.2	-0.2	0.3
100	77.1	76.8	77.1	76.9	76.9	-0.3	0.0	-0.2	-0.2
130	122.6	122.4	122.6	122.4	122.2	-0.2	0.0	-0.2	-0.4
150	157.6	157.3	157.6	157.4	157.1	-0.3	0.0	-0.2	-0.5
190	237.4	237.3	237.5	237.2	236.5	-0.1	0.1	-0.2	-0.9
220	305.2	304.9	305.1	304.8	305.2	-0.3	-0.1	-0.4	0.0

4.3 The integral depth-dose curves

Figure 4.2 shows a comparison of the integral depth-dose curves acquired with all chambers from 70 to 220 MeV. The largest deviation between curves was located between the entrance plateau and proximal rise of the Bragg peak. We found that IBA Giraffe has a variation in curve arrangement in each energy as shown in figure 4.3 that could be explained by the different conditions of IBA Giraffe compared to the other chambers as it is MLIC and inside is water-equivalent material. Moreover, the curve of 70 MeV has a large variation due to a water ripple

effect caused by the shallow depth, 3 mm step size, and large detector diameter, especially for PTW Bragg peak chamber type 34089.

There are the same curve arrangements for 130, 150, 190, and 220 MeV. As in figure 4.4, the highest curve is from PTW Bragg peak chamber type 34089 (BP15) with 15 cm diameter, followed by IBA Giraffe with 12 cm diameter, PTW Bragg peak chamber type 34070 (BP8), and PTW PeakFinder with 8 cm diameter. PTW PeakFinder has lower curves than PTW Bragg peak chamber type 34070, which could be explained by the smaller volume of water, which could lead to less scatter.

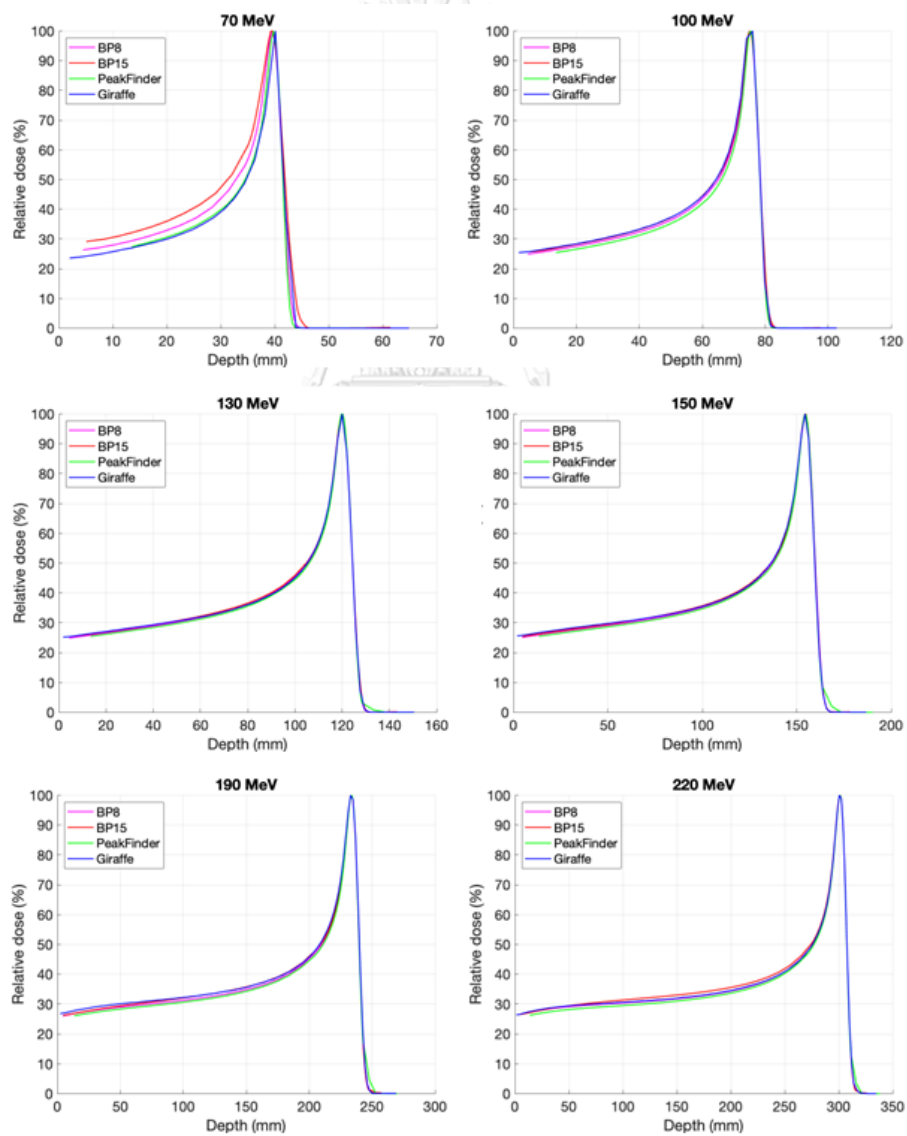


Figure 4.2 The integral depth dose curves acquired with all chambers for proton beam energies of 70, 100, 130, 150, 190, and 220 MeV.

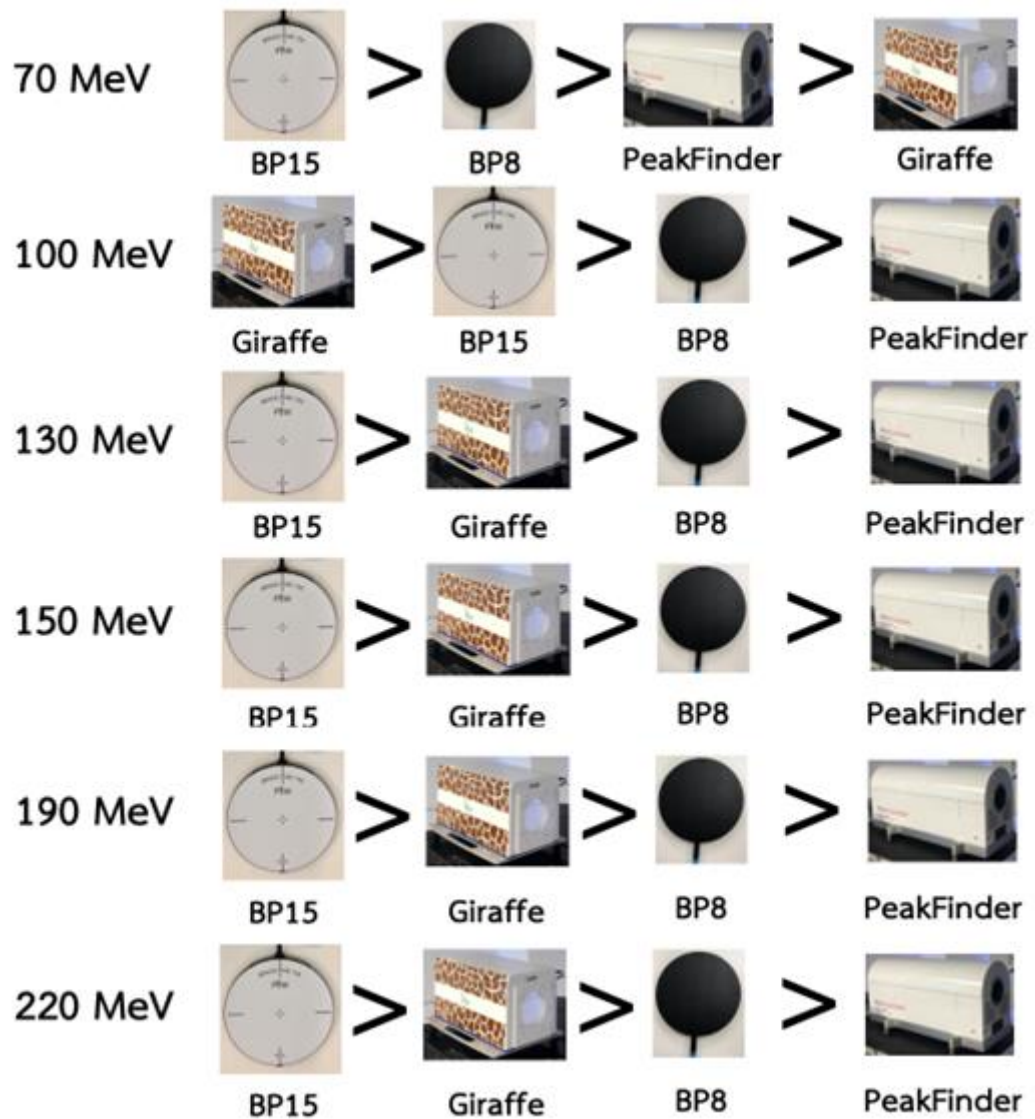


Figure 4.3 The curve arrangements of all chambers in the largest deviation region.

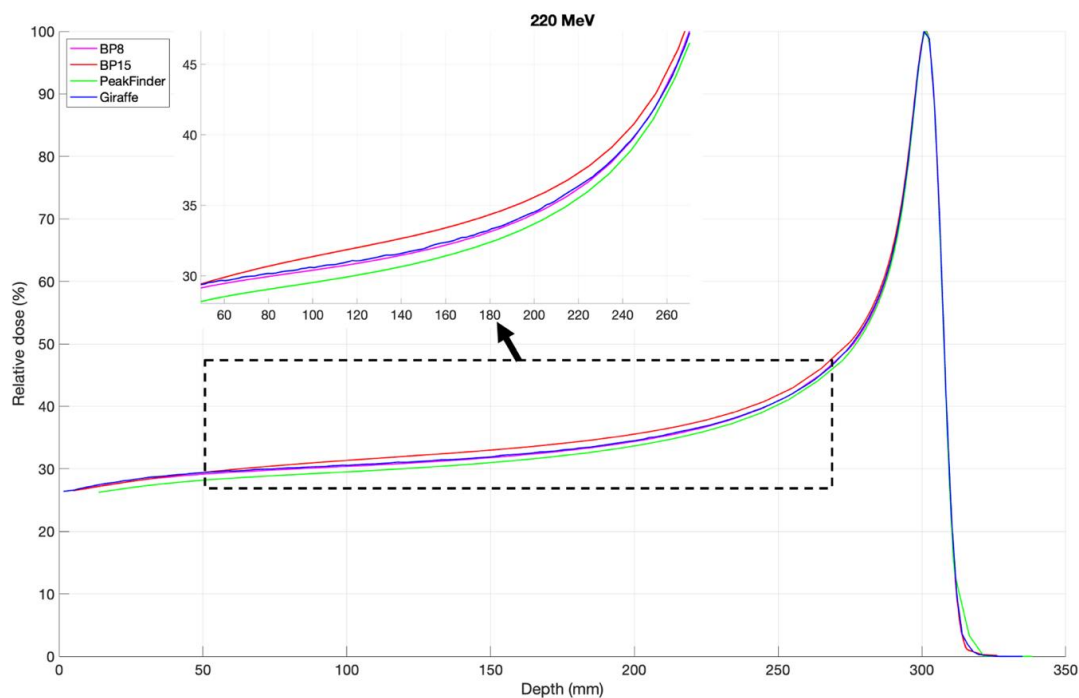


Figure 4.4 The integral depth dose curves acquired with all chambers of 220 MeV.

4.4 The geometrical collection efficiency

The integral depth-dose curves of 130, 150, 190, and 220 MeV were interpolated on a 1 mm grid and scaled in-depth to match R_{80} from NIST before calculating the ratio of each energy. The proportions of a depth-dose curve acquired with two types of PTW Bragg peak chambers are shown in figure 4.5. At the intermediate depth, we found that PTW Bragg peak chamber type 34089 with the largest diameter had an increased collection efficiency compared to PTW Bragg peak chamber type 34070 of about 1.4%, 1.6%, 2.7%, and 3.8% for 130, 150, 190, and 220 MeV, respectively. Figure 4.6 shows the ratio of a depth-dose curve acquired with PTW PeakFinder and PTW Bragg peak chamber type 34089. We also found that PTW Bragg peak chamber type 34089 had an increased collection efficiency than PTW PeakFinder of about 2.9%, 3.0%, 4.5%, and 6.1% for 130, 150, 190, and 220 MeV, respectively. Figure 4.7 shows the ratio of a depth-dose curve acquired with IBA Giraffe and PTW Bragg peak chamber type 34089. We also found that PTW Bragg peak chamber type 34089

increased collection efficiency compared to IBA Giraffe by about 0.8 %, 0.2%, 0.1%, and 3.1% for 130, 150, 190, and 220 MeV, respectively. Table 4.9 summarizes the geometrical collection efficiency of 130, 150, 190, and 220 MeV.

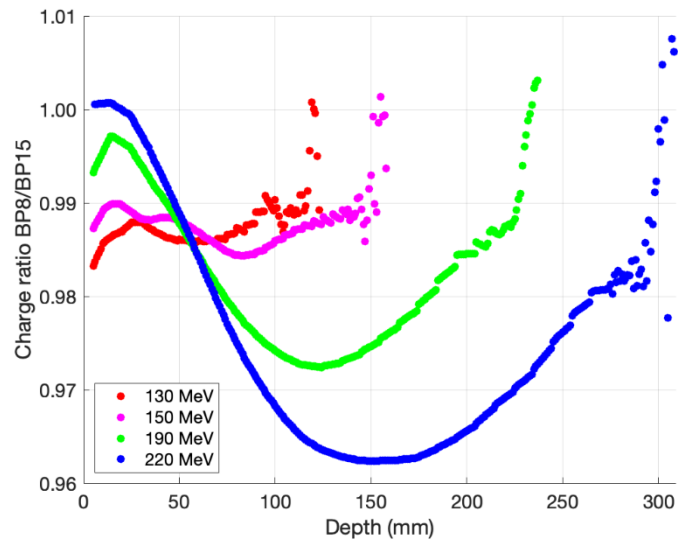


Figure 4.5 The ratios of depth-dose curves acquired with two types of PTW Bragg peak chamber 34070 and 34089.

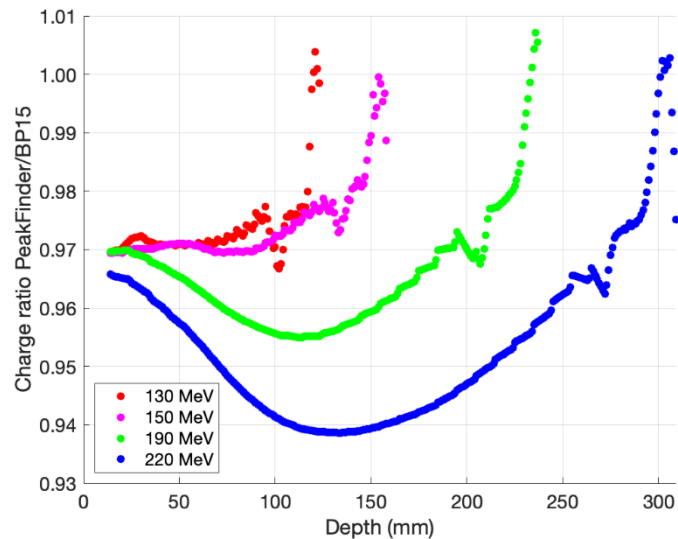


Figure 4.6 The ratios of depth-dose curves acquired with PTW PeakFinder and Bragg peak chamber 34089.

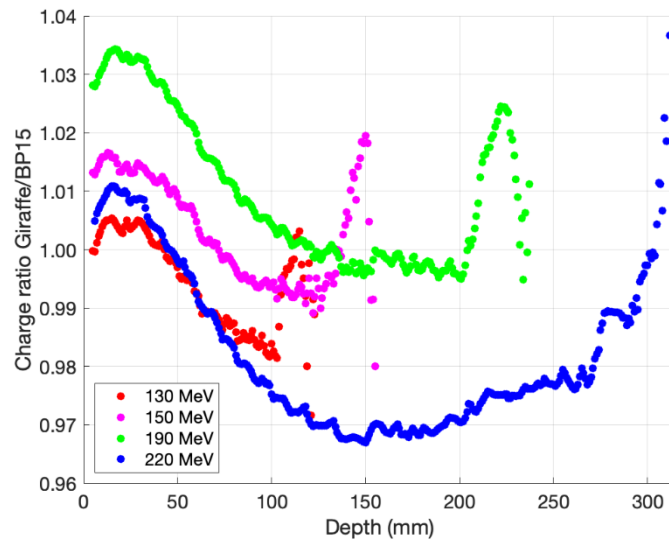


Figure 4.7 The ratios of depth-dose curves acquired with IBA Giraffe and PTW Bragg peak chamber 34089.

Table 4.9 Geometrical collection efficiency (%) of 130, 150, 190, and 220 MeV

Energy (MeV)	Geometrical collection efficiency (%)		
	BP8/BP15 (8 cm/15 cm diameter)	PeakFinder/BP15 (8 cm/15 cm diameter)	Giraffe/BP15 (12 cm/15 cm diameter)
130	1.4	2.9	0.8
150	1.6	3.0	0.2
190	2.7	4.5	0.1
220	3.8	6.1	3.1

CHAPTER 5

DISCUSSION AND CONCLUSION

5.1 Discussion

The characteristics of the detectors for short-term reproducibility, linearity, and repetition rate dependence indicated that all chambers were suitable for the proton beams measurement. Furthermore, R_{80} differences were within tolerance, indicating that all chambers can accurately measure the Bragg peak range (R_{80}). The IBA Giraffe's resolution of 2 mm could explain a maximum difference of R_{80} at 190 MeV. For the integral depth-dose curve measurements, the larger diameter detector has a higher curve in the plateau region due to the halo effect. However, the curve of the PTW PeakFinder is lower than the PTW Bragg peak chamber type 34070 for the same 8 cm diameter. However, when compared to Grevillot et al. (18) by normalized dose at 130 mm depth. We realized that there is a good agreement because the curves of the PTW PeakFinder and Bragg peak chamber type 34070 also have similar shapes in the plateau region.

PTW Bragg peak chamber type 34070, PTW PeakFinder, and IBA Giraffe, PTW Bragg peak chamber type 34089 with the largest diameter could improve geometrical collection efficiency by 1.4% to 3.8%, 2.9% to 6.1%, and 0.8% to 3.1%, respectively. The most significant difference was found at intermediate depths and the highest proton energy. Therefore, the increasing chamber diameter has improved geometrical collection efficiency depending on beam energy and depth. It means that the PTW Bragg peak chamber type 34089 with the largest diameter could collect more secondary proton from the halo, which is mainly produced by nuclear and coulomb interactions with the detection medium, and these agreed with Baumer C et al. (4), Langner UW et al. (2), and Mojzeszek N et al. (13). The ratios between two chamber types in the peak region were close to one, indicating less halo effect, whereas higher collection efficiencies were observed at the distal fall-off region due to the limitation of detectors at the high dose gradient and step size of 5 mm.

The results obtained agreed with Baumer C et al. (4) who reported the collection efficiency up to 2.0% and 3.5% between PTW Bragg peak chamber type 34070 and IBA Stingray chamber for 180 and 226.7 MeV, respectively. In addition, Mojzeszek N et al. (13) achieved a higher collection efficiency of 5.8% between chamber diameters of 8 and 40 cm for 226.08 MeV by using data assessed with Monte Carlo calculations. The diameter of the chamber that those authors used to compare with the 8 cm chamber diameter could explain these differences. For this research, we used a newly designed large-area ionization chamber with a 15 cm diameter.

5.2 Conclusion

The integral depth-dose curves of proton pencil beams are acquired with four different detectors. The results show that PTW Bragg peak chamber type 34089, with a 15 cm diameter, has increased geometrical collection efficiency up to 3.8%, 6.1%, and 3.1% compared to PTW Bragg peak chamber type 34070, PTW PeakFinder, and IBA Giraffe, respectively for the highest energy. This research was concluded that a larger plane-parallel ionization chamber could increase the geometrical collection efficiency of the detector, especially at intermediate depths and high-energy proton beams, and less difference in the Bragg Peak region. PTW PeakFinder and IBA Giraffe have limitations in the measurement; therefore, they should be used mainly for fast quality assurance and should not be introduced into a treatment planning system as the input data.

REFERENCES

1. Newhauser WD, Zhang R. The physics of proton therapy. *Phys Med Biol*. 2015;60(8):R155-209.
2. Langner UW, Eley JG, Dong L, Langen K. Comparison of multi-institutional Varian ProBeam pencil beam scanning proton beam commissioning data. *J Appl Clin Med Phys*. 2017;18(3):96-107.
3. Farr JB, Moyers MF, Allgower CE, Bues M, Hsi WC, Jin H, et al. Clinical commissioning of intensity-modulated proton therapy systems: Report of AAPM Task Group 185. *Med Phys*. 2021;48(1):e1-e30.
4. Baumer C, Koska B, Lambert J, Timmermann B, Mertens T, Takoukam Talla P. Evaluation of detectors for acquisition of pristine depth-dose curves in pencil beam scanning. *J Appl Clin Med Phys*. 2015;16(6):151-63.
5. Gottschalk B, Cascio EW, Daartz J, Wagner MS. On the nuclear halo of a proton pencil beam stopping in water. *Phys Med Biol*. 2015;60(14):5627-54.
6. Kempe J, Gudowska I, Brahme A. Depth absorbed dose and LET distributions of therapeutic ¹H, ⁴He, ⁷Li, and ¹²C beams. *Med Phys*. 2007;34(1):183-92.
7. Safai S. Dose Delivery Verification. *arXiv: Medical Physics*. 2017:49.
8. Benefits of Intensity Modulated Proton Therapy [Internet]. [cited 2022 Jan 10]. Available from: <https://www.varian.com/products/proton-therapy/benefits-intensity-modulated-proton-therapy>.
9. Vitti ET, Parsons JL. The Radiobiological Effects of Proton Beam Therapy: Impact on DNA Damage and Repair. *Cancers (Basel)*. 2019;11(7).
10. Module 3: Equipment for Proton Therapy Delivery [Internet]. [cited 2022 Jan 9]. Available from: <https://www.oncolink.org/healthcare-professionals/oncolink-university/proton-therapy-professional-education/oncolink-proton-education-modules/module-3-equipment-for-proton-therapy-delivery>.
11. Schätti A, editor *Towards the treatment of moving targets with scanned proton beams* 2013.
12. St. James S, Grassberger C, Lu H-M. Considerations when treating lung cancer

with passive scatter or active scanning proton therapy. Translational lung cancer research. 2018;7 2:210-5.

13. Mojzeszek N, Klodowska M, Komenda W, Stolarczyk L, Kopec R, Olko P. Geometrical Efficiency of Plane-Parallel Ionization Chambers in Proton Scanning Beam. Radiat Prot Dosimetry. 2018;180(1-4):334-7.

14. MP3-P and MP3-PL Water Phantom [Internet]. [cited 2021 Apr 10]. Available from: <https://www.ptwdosimetry.com/products/mp3-ppl/?L=0>.

15. Vai A, Mirandola A, Magro G, Maestri D, Mastella E, Mairani A, et al. Characterization of a MLIC Detector for QA in Scanned Proton and Carbon Ion Beams. Int J Part Ther. 2019;6(2):50-9.

16. Stopping-Power & Range Tables for Electrons, Protons, and Helium Ions [Internet]. [cited 2022 Jan 10]. Available from: <http://www.nist.gov/pml/data/star>.

17. Arjomandy B, Taylor P, Ainsley C, Safai S, Sahoo N, Pankuch M, et al. AAPM task group 224: Comprehensive proton therapy machine quality assurance. Med Phys. 2019;46(8):e678-e705.

18. Grevillot L, Stock M, Palmans H, Osorio Moreno J, Letellier V, Dreindl R, et al. Implementation of dosimetry equipment and phantoms at the MedAustron light ion beam therapy facility. Med Phys. 2018;45(1):352-69.



จุฬาลงกรณ์มหาวิทยาลัย
CHULALONGKORN UNIVERSITY

VITA

NAME Phatthraporn Thasasi

DATE OF BIRTH 22 June 1997

PLACE OF BIRTH Bangkok, Thailand

INSTITUTIONS ATTENDED - Bachelors in Radiological Technology, Faculty of Allied Health Sciences, Chulalongkorn University, Bangkok, Thailand
- Master of Science in Medical Physics, Faculty of Medicine, Chulalongkorn University, Bangkok, Thailand
- Division of Radiation Oncology, Department of Radiology, King Chulalongkorn Memorial Hospital, Bangkok, Thailand

PUBLICATION Phatthraporn T, Sirinya R, Puntiva O, Sornjarod O. Assessment of geometrical collection efficiency in proton pencil beam scanning using plane-parallel ionization chambers in Proceedings of 19th South-East Asia Congress of Medical Physics (SEACOMP) - 13th Annual Meeting of Thai Medical Physicist Society (TMPS) - 14th Annual ASEAN College of Medical Physics (ACOMP), Phuket, Thailand, 2021

